High Pressure Research

An International Journal

ISSN: (Print) (Online) Journal homepage: https://www.tandfonline.com/loi/ghpr20

Development of a high pressure stirring cell up to 2 GPa: a new window for chemical reactions and material synthesis

Ying-Jui Hsu, Alisa Gordeeva, Mathis Antlauf, Ulrich Häussermann & Ove Andersson

To cite this article: Ying-Jui Hsu, Alisa Gordeeva, Mathis Antlauf, Ulrich Häussermann & Ove Andersson (2020) Development of a high pressure stirring cell up to 2 GPa: a new window for chemical reactions and material synthesis, High Pressure Research, 40:3, 358-368, DOI: 10.1080/08957959.2020.1775200

To link to this article: https://doi.org/10.1080/08957959.2020.1775200

Published online: 05 Jun 2020.

HIGH PRESSURE RESEARCH
2020, VOL. 40, NO. 3, 358–368
https://doi.org/10.1080/08957959.2020.1775200

Taylor & Francis
Taylor & Francis Group

Development of a high pressure stirring cell up to 2 GPa: a new window for chemical reactions and material synthesis

Ying-Jui Hsu[a], Alisa Gordeeva[b], Mathis Antlauf[a], Ulrich Häussermann[b] and Ove Andersson[a]

[a]Department of Physics, Umeå University Umeå, Sweden; [b]Department of Materials and Environmental Chemistry, Stockholm University Stockholm, Sweden

ABSTRACT

A new method for stirring under high pressure conditions has been developed and tested. The key component is a Teflon cell assembly equipped with magnetic stirring function, which is capable to operate across a wide pressure range, up to at least 2 GPa, in a large volume press. The setup enables adjustable stirrer rotation rate and detection of stirring in a sample, *e.g.* to observe liquid–solid phase transitions at high pressure. The viscosity limit of stirring is ca. 500 times that of water at room temperature (*i.e.* ~500 mPas). Moreover, we show that zinc oxide nanoparticles hydrothermally synthesized at 0.5 GPa and 100°C under stirring conditions show an order of magnitude smaller size (100 nm) compared to those synthesized under non-stirring conditions (1 μm). The wide pressure range for stirring of viscous media opens interesting possibilities to produce novel materials via hydrothermal synthesis and chemical reactions.

ARTICLE HISTORY
Received 1 March 2020
Accepted 23 May 2020

KEYWORDS
Magnetic stirring; hydrothermal synthesis; high pressure; metal oxide

1. Introduction

Stirring is an effective means to equalize concentration and temperature gradients during chemical reactions and, thus, is essential for the agitation of heterogeneous reactions. In particular, stirring is essential for almost all organic reactions that involve solvents. Stirring has also been widely applied in hydrothermal synthesis used in the ceramic capacitor industry [1,2] semiconductor production [3], optoelectronic devices [4,5], and production of electrode materials for Li-ion batteries [6]. Continuous stirring effectively prevents settling and aggregation of nanoparticles in solution, which is, *e.g.* required to attain high-quality quartz [7]; stirring speed can also be an important parameter for finding optimized crystal growth conditions [5,6].

In laboratory settings one usually distinguishes between magnetic stirring, using a magnetic stir bar, and mechanical stirring. The latter is more efficient for highly viscous mixtures. When extending solvent-based/assisted chemical reactions to gigapascal high pressure conditions typically piston cylinder devices are applied [8]. Attempts have been made to combine mechanical stirring with piston cylinder high pressure cells.

CONTACT Ove Andersson ove.b.andersson@umu.se Department of Physics, Umeå University, 901 87 Umeå, Sweden

However, with mechanical stirring maximum pressures attainable appear to be limited to 0.3 GPa [8,9]. In contrast, magnetic stirring should allow for much higher pressures, in the gigapascal range. To the best of our knowledge, combining piston cylinder cells with a magnetic stirring capability has never been pursued. An increased pressure range for stirring of viscous media therefore opens up for new possibilities to produce novel materials via solvent-based reactions.

Therefore, we have designed and tested a high pressure cell equipped with stirring function; the cell has capacity to operate up to at least 2 GPa for temperatures up to ca. 200°C in a large volume press. Our setup enables adjustable magnetic stirrer rotation rate (*i.e.* frequency) and monitoring of stirring of a sample; it can therefore be used to observe phase transitions at high pressure, *e.g.* liquid to solid transitions upon compression. Here, we report details of the high pressure cell and electronics, the viscosity limit for stirring, as well as an example on the morphology of zinc oxide synthesized under stirring and non-stirring hydrothermal conditions at high pressure.

2. Design and test of high pressure stirring cell

2.1. High pressure stirring cell

The high pressure stirring cell was designed for a piston-cylinder-type of pressure vessel of 45 mm internal (bore) diameter (Figure 1) with the load supplied by a hydraulic press. The

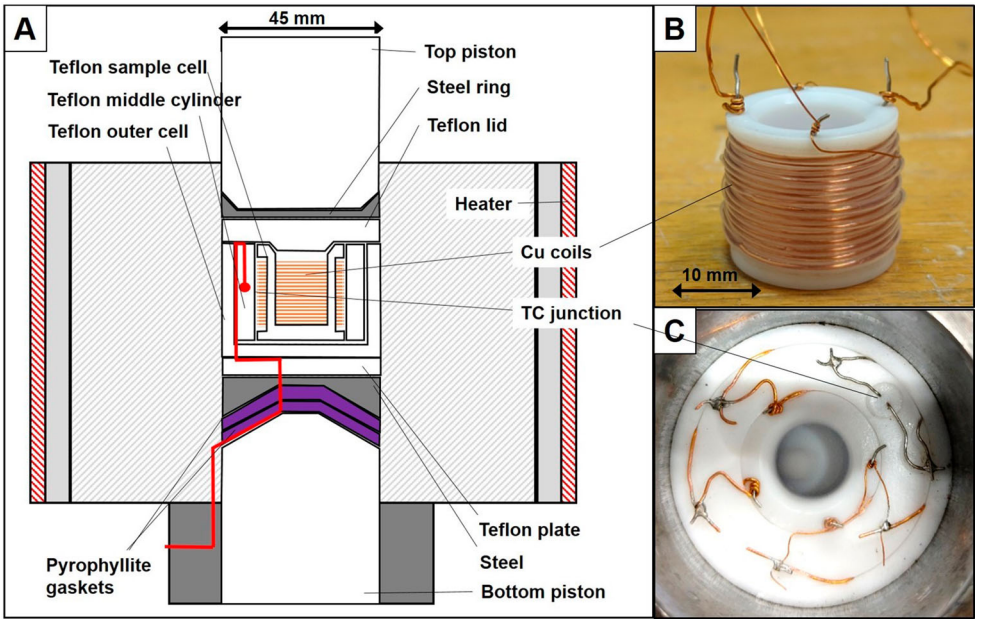

Figure 1. (A) Schematic drawing of the cross-section of the cell assembly mounted in a high pressure piston-cylinder device with top and bottom pistons. (B) The sample cell equipped with two Cu coils in a stacked coil design for stirring and detection of stirring; the enamel-coated Cu wires are extra-insulated with Teflon tubing. (C) Top-viewed of cell assembly showing the thermocouple (TC) position and Cu coils. (The compound construction of the pressure vessel is not illustrated in the figure – see text in section 2.1 for details.)

pressure vessel, with ca. 3 GPa capacity, is a compound construction of two hollow cylinders; an inner cylinder (hardened to ca. 63 HRC) of 100 mm height, 45 mm inner diameter and 105.0 mm outer diameter (on the upper side). The outer part of the cylinder is slightly conically shaped (1°) and the cylinder was press-fitted into a conical (1°) inner part of another cylinder (hardened to ca. 51 HRC) of 100 mm height, 104.2 mm inner diameter (on the upper side) and 250 mm outer diameter. The compound construction is surrounded by a steel ring (splinter guard). With this construction, compressive forces from the outer cylinder support the inner cylinder. The sample cell was a Teflon cylinder of 24 mm in outer diameter, 13 mm in internal diameter and 18 mm in height (Figure 1 (B)). It was equipped with two coils, a primary coil and a signal pick-up coil, which were wound with enamel coated copper wires: 0.55 and 0.2 mm in diameter for primary and pick-up, respectively. The wires were inserted in Teflon tubing for additional insulation between the coils, which were made in stacked coil design. (Without Teflon tubing, the coils occasionally became shortcut on heating at 2 GPa.) The sample cell assembly was inserted into a Teflon cylinder of 25 mm in internal diameter, which served as an insulation layer between the coils and the thermocouple and electrical feedthroughs (0.4 mm in diameter Cu-wires). The cell (and cylinder) was thereafter inserted in a larger Teflon container of 39 mm internal diameter. The sample cell was sealed with a Teflon lid and tightly fitted into a piston-cylinder apparatus and thereafter the whole cell assembly was transferred into a 1500 ton hydraulic press, which supplied the load. The pressure in the cell was determined from the signal of an oil pressure gauge, which had previously been calibrated with an uncertainty of ±0.05 GPa (at 2 GPa) in a separate experiment by using the pressure dependence of the resistance of a manganin wire. Temperature was varied by heating the whole pressure vessel using an external resistive heater, and it was measured by an internal chromel-alumel thermocouple with an estimated temperature uncertainty of ±1 K. (The thermocouple was immersed in pure water so that the pressure could also be verified from the ice VI melting curve.) Typically, samples were compressed at a rate of 0.3 GPa/h and heated at 0.3 K/min. A schematic illustration of the cell assembly is shown in Figure 1.

The electric circuit of the setup is illustrated in Figure 2. The circuit is designed to generate a magnetic field by the primary copper coil that is strong enough to drive a stirrer magnet in the sample cell under high-temperature high pressure conditions. The AC current in the primary coil is supplied by a power amplifier (Kepco BOP 72-5m) whose frequency and voltage are controlled by a function generator. A current limiting resistor (2.5 Ω) is mounted in series with the coil for circuit protection. (The 2.5 Ω resistor was

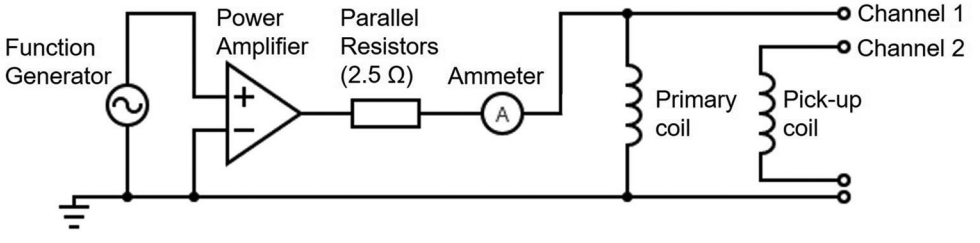

Figure 2. The electric circuit of the setup.

made from four 10 Ω, 50 W, resistors, connected in parallel and mounted on a Cu block for heat dissipation.) To monitor movements of the magnet, the signal from the pick-up coil is connected to an oscilloscope (Agilent DSO6012A).

2.2. Optimization of cell design

To optimize magnetic stirrer performance under high pressure and temperature conditions, the shape of the magnet, the choice of magnet material, magnetic field (current), and frequency are important parameters. With the volume and geometry of the sample cell and coil design used here, we found that egg-shaped, cubic and ball types of magnets perform well. Moreover, a test showed that sintered NdFeB magnets (grade N35EH with a maximum service temperature of 200°C at atmospheric pressure) have sufficient tolerance towards high-temperatures to stir a relatively viscous slurry up to at least 130°C at 2 GPa. (At this temperature, stirring stopped possibly due to demagnetization, a precipitation reaction or partial sample cell collapse.) The magnetic field inside a current-carrying (long) coil is determined by Ampère's law, $B = \mu_0 * n * I$, where B is the magnetic field (magnetic flux density), μ is the magnetic permeability of free space, n is the number of loops per unit length and I is the current. Consequently, at a fixed length of the coil, which is determined by the cell design, the magnetic field is proportional to the number of loops and current. In other words, the more number of loops, the less current is required to drive the magnetic stirrer, which reduces Joule heating and, therefore, the uncertainty of the temperature inside the sample cell. With this in consideration, a current of 0.5–3 A and frequency ranging from 2 to 80 Hz (*i.e.* 120–4800 rpm) gave optimized stirring performance for the liquid media (oil and water) used in our study.

Still, in order to accurately determine the temperature in the sample cell, we measured the temperature difference (ΔT) due to Joule heating and stirring between a thermocouple positioned inside the sample cell and one at the position shown in Figure 1(C). The experiments showed that the time constant of the setup is about 30 min. That is, after start of stirring (current), ΔT increased significantly during the first 30 min and reached a plateau after ca. 90 min. Figure 3 shows that ΔT has a positive linear correlation with applied power at atmospheric pressure. When the cell was pressurized to 2 GPa, the temperature gradient in the cell decreased to less than half the value measured under ambient conditions, which is due to improved thermal contact and about 3 times higher thermal conductivity of Teflon [10]. The radial temperature gradient was determined by two thermocouples positioned at different distances from the sample; for a typical current required for stirring, corresponding to about 0.4 W, these indicated a difference of ±1 K or less at 2 GPa. The calibration result, which shows that the measured temperature is about 1.5 K less than the sample temperature, was later used to calculate the sample temperature during all synthesis experiments. It should be noted that the forced liquid convection by stirring effectively eliminates temperature differences in the sample.

2.3. Stirring of a high viscosity liquid

As the viscosity of a liquid increases, *e.g.* due to increasing pressure or mixing, stirring becomes increasingly more difficult. To determine the viscosity limit of stirring and its

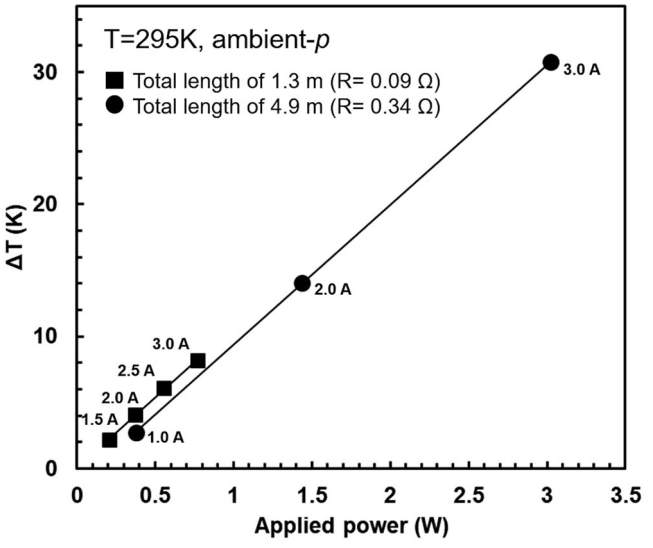

Figure 3. Temperature difference between a thermocouple positioned inside the sample cell and one at the position shown in Figure 1(C) plotted against power at ambient conditions. The results are for two different coils: coil 1 with 20 turns and 14 mm in height (■), and coil 2 with 73 turns and 24 mm in height (●). The applied current is shown next to data points.

dependence on stirring rate, we have studied a commercial oil (Shell Morlina S2 B 150 oil used for industrial bearing and circulating oil system applications) with well-documented physical and chemical properties [11]. Tests to stir were done by varying frequency and current at three different temperatures (viscosities); in this case a samarium-cobalt magnet (PTFE stirring bar, Oval Rare Earth, 10 × 5 mm) was used. The test results are summarized in Figure 4. At the highest test viscosity of $\eta = 470$ mPa s, stirring requires high current, ~3 A, and a frequency below 5 Hz. At medium viscosity of $\eta = 78$ mPa s, the current must exceed 1.5 A, and then it is possible to stir at frequencies below 50 Hz. At the lowest test viscosity, $\eta = 12$ mPa s, the magnetic stirrer performs well with a current of 1 A for frequencies up to 50 Hz for a coil with 20 turns and 14 mm in height (Figure 1(B)). Our results show that for water-based hydrothermal synthesis experiments, our setup is capable to stir up to the freezing pressure of water at room temperature; the viscosity of water initially decreases with increasing pressure, but it increases above 0.05 GPa [12], and further increases to about 3 mPa s at 1 GPa [13–15].

2.4. Sample characterization

Materials synthesized under non-stirring and stirring hydrothermal conditions were characterized by ambient temperature powder X-ray diffraction (XRD) on a Panlytical X'Pert Alpha1 diffractometer operated with Cu$K\alpha_1$ radiation (45 kV and 40 mA) and a scan speed of 0.012° min^{-1} in 2θ diffraction geometry. Powder samples were mounted on a Si wafer zero-background holder and diffraction patterns measured in a 2θ range 10–80°. Scanning electron microscopy (SEM) and transmission electron microscopy (TEM) were used to examine the particle size and morphology. The synthesized products,

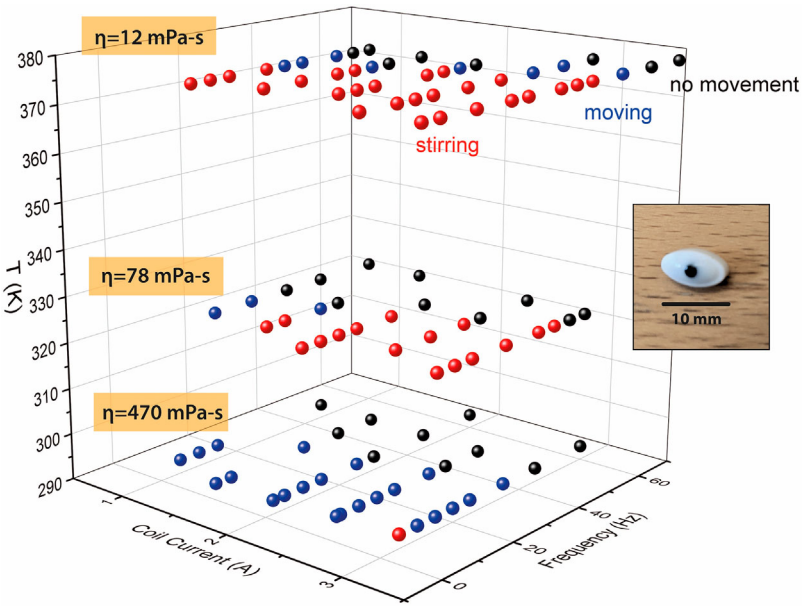

Figure 4. Current and frequency ranges for stirring of a commercial pump oil at atmospheric pressure using a samarium-cobalt magnet (PTFE stirring bar, Oval Rare Earth, 10 × 5 mm – see inset) at three different viscosities, as indicated. The results correspond to a coil with 20 turns and the dimensions given in Figure 1(B) (14 mm in height). (Note that the viscosity range of stirring can be increased by using a stronger magnet, higher current and more turns in the coil, but the two latter options increase the cell temperature.)

in the form of powders, were mounted on stubs using carbon tape for SEM analysis. For TEM analysis, a JEOL JEM 2100 field emission microscope operating at 200 kV was used, and samples were dispersed in ethanol and deposited on holey carbon films supported by copper TEM grids.

3. Proof of concept

3.1. Detection of liquid water–ice phase transition by stirring signals at high pressure

The new setup allows for real-time observations of transformations that changes the sample fluidity and, in principle, a rough estimate of the viscosity through the signal from the pick-up coil. It is particularly useful to monitor when a liquid phase crystallizes to a solid phase and vice versa during compression/decompression and heating/cooling processes throughout an experiment. Moreover, if the signal from the pick-up coil indicates that stirring has stopped, or has become less intense, then current and/or frequency can be adjusted to restart and optimize stirring. It should be noted that in the high pressure cell, stirring can be applied immediately after loading sample solution to ensure homogeneity and avoid precipitation and/or layers separation occurring in the liquid solution.

To illustrate detection of transitions upon compression and heating, we use pure water as an example; water was pressurized to 2 GPa at room-T, *i.e.* it was pressurized deep in to the stability range of ice VI. (To avoid phase separation in studies of water solutions, crystallization can be prevented by a suitable pressure-temperature route that keeps the solution above the ice VI crystallization boundary.) As shown in Figure 5(A), the signal from the pick-up coil indicated stirring up to 1.10 GPa at 295 K ('stirring signal'), but it changed abruptly at 1.15 GPa to a form suggesting a non-moving magnet ('static signal'); this indicates that liquid water crystallized to ice VI at 1.15 GPa in agreement with an exothermic transition concurrently recorded by the thermocouple (Figure 5(C)). On further pressurization to 2 GPa, the signal of the pick-up coil remained unchanged. Upon heating at 2 GPa, the signal remained static up to 348 K; the first stirring signal was recorded at 349 K, indicating that the sample transformed from a solid to a liquid between 348 and 349 K (Figure 5(B)). The transition temperature corresponds well to the melting temperature of 348–349 K (Figure 5(D)) deduced from the equilibrium phase line between ice VI and liquid water at 2 GPa [16]. At this transition, which occurs at equilibrium, it was harder to determine the transition temperature from the thermocouple signal.

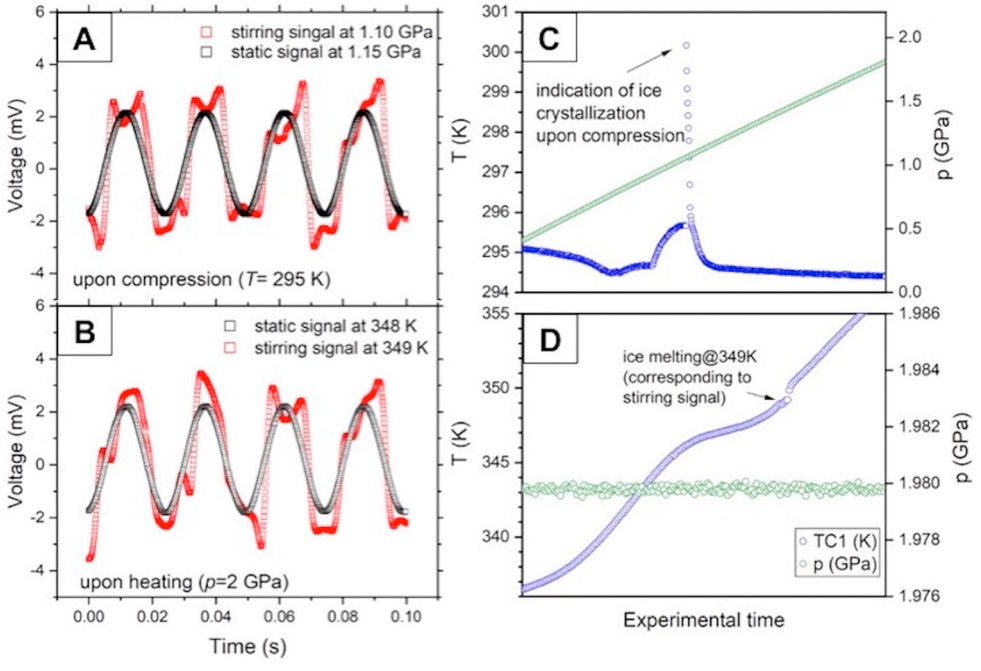

Figure 5. Acquired signals upon compression and, subsequent, heating of water. (A) Stirring signals recorded from ambient pressure up to 1.10 GPa show that the sample was in liquid form. The first static signal was detected at 1.15 GPa, indicating ice crystallization. (B) Upon heating at 2 GPa, static signals recorded from 295 to 348 K show that the sample was in a solid state. The first stirring signal was detected at 349 K, indicating ice melting. (C) An exothermic peak recorded from a thermocouple indicated ice crystallization at around 1.1–1.15 GPa and 295 K, in a good agreement with the signal from the pick-up coil. (D) Upon heating at 2 GPa, the thermocouple signal shows a feature at 349 K that suggests ice melting. The applied coil current was ca. 0.6 A and the frequency 40 Hz.

3.2. The effect of stirring on morphology of wurtzite-ZnO particles

The effect of stirring on the morphology under the pressure of changed water properties, and therefore higher viscosity/internal friction as well as other changes, was exploited by hydrothermal synthesis of wurtzite-ZnO (w-ZnO) particles. Here we show an example of hydrothermal conversion of ε-$Zn(OH)_2$ to w-ZnO with and without magnetic stirring at 0.5 GPa and 100°C. The frequency of the stirring experiment was set at 30 Hz (*i.e.* 1800 rpm). Both experiments resulted in w-ZnO particles after 2 h treatment; however, stirring during hydrothermal synthesis of w-ZnO caused distinct changes in particle size and morphology. The TEM images show that synthesis under stirring produces plate-shaped particles (Figure 6(B)) whereas needle-shaped particles form under non-stirring conditions (Figure 6(A)). Moreover, the TEM results confirm that stirring reduces the average size of w-ZnO particles by about an order of magnitude, from 1-5 to 0.1–0.5 μm, in good agreement with the X-ray results (Figure 6(C)). The patterns show that the three main peaks, (100), (002) and (101), of the stirred sample are broader compared to those of the non-stirred sample. This suggests that stirring is favorable for obtaining small particles with uniform size distribution and our results are consistent with several previous studies [1,17]. In addition, because of the particle size reduction, stirring effectively increases the surface to volume area of the particles. This results in higher reactivity and thus better performance in applications such as catalytic processes. Indeed, we found a much larger specific surface area (BET) of 40.5 $m^2\ g^{-1}$ for the stirred w-ZnO powder in comparison to that of the non-stirred sample (<1.0 $m^2\ g^{-1}$). This suggests that without stirring large and aggregated particles are formed, in good agreement with the TEM and X-ray results.

Hydrothermal conversion of ε-$Zn(OH)_2$ to ZnO has previously been studied extensively under subcritical to supercritical conditions, *i.e.* at pressures below 300 bar, using

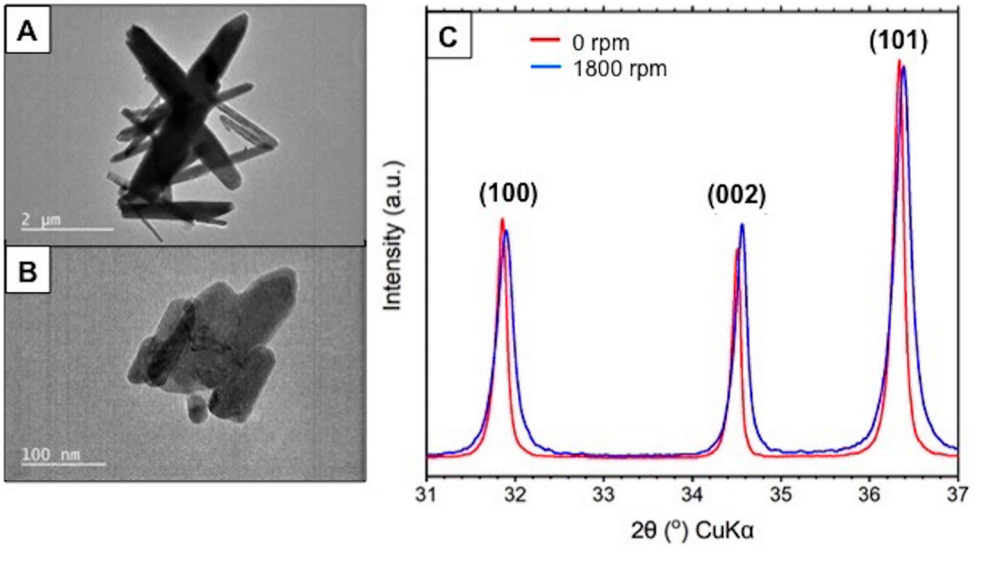

Figure 6. TEM images of w-ZnO samples synthesized at 0.5 GPa and 100°C by hydrothermal treatment under (A) non-stirring and (B) stirring conditions. (C) Stirring resulted in broader XRD peaks because of smaller crystal sizes.

autoclaves; it was shown that particle size and morphology can be tuned by varying parameters such as pressure, temperature, reaction time and pH [18–20]. In an experiment without stirring, Demoisson et al. [18] showed that the size of as-produced needle-shaped particles increased from 0.2 μm to 0.5–1 μm when the pressure of the synthesis increased from 2 bar (at 86°C) to 300 bar (at 98°C). This is in qualitative agreement with the finding here of needle shaped-particles of sizes in the 1–5 μm range after synthesis under non-stirring conditions at 5000 bar and 100°C. These results suggest that an isothermal pressure increase promotes hydrothermal synthesis of larger ZnO-particles.

The stirring frequency is also an important parameter for the nucleation/growth kinetics of different hydrothermal routes of materials [5,6]. In particular, Kuo et al. [5] showed that it is possible to use stirring for shaping the tips of hydrothermally grown ZnO nano-rods; they reported that the stirring speed affected the dimensions and shape of the ZnO nanostructures. Although not tested here, the setup can be used to investigate the effect of stirring rate on particle growth under high pressure. The setup has been tested for stirring between 120 and 4800 rpm, but the results for the morphology and particle size refer only to synthesis under stirring at 1800 rpm using a cubic-shaped magnet. We can conclude that despite the simple cell design with only 180 degrees flipping of the magnetic field and a cubic magnet, the morphology of the as-synthesized ZnO was significantly affected by synthesis under stirring conditions. Thus, our study illustrates the potential of future stirring experiments at high pressures utilizing changes in water/solvent properties, *e.g.* viscosity and dielectric properties, and changes in stability ranges of phases for producing interesting materials.

4. Conclusion

A new experimental setup with stirring function was designed and tested for high pressure hydrothermal synthesis. The setup fits in a piston-cylinder device of 3 GPa capacity and it was tested up to 2 GPa. The sample cell, with a sample volume up to ca. 2.5 cm^3, was constructed from Teflon; in combination with external heating, it limits the maximum temperature to 200–250°C. The stirring rate can be adjusted between 120 and 4800 rpm, and the magnet movement is monitored; this enables tests to optimize and control the growth of particles by adjustment of stirring speed. Moreover, the monitoring function enables the detection of liquid–solid phase transitions. A test to synthesize wurtzite-ZnO under stirring conditions produced smaller (100–500 nm) and more uniform particles than corresponding synthesis without stirring, which yielded aggregated particles with sizes in the 1–5 μm range.

The setup presented here opens up an increased pressure range for stirring of various media and therefore new possibilities for producing novel materials via solvent-based synthesis schemes and chemical reactions. This includes especially hydrothermal conversions and reactions at gigapascal pressures as well as organic reactions in fluids [21–23].

Acknowledgements

This work was funded by The Swedish Research Council (Grant 2016-04413). We gratefully acknowledge the financial supports from Kempestiftelserna (MA) and Stiftelsen Olle Engkvist Byggmästare (YJH).

Disclosure statement

No potential conflict of interest was reported by the author(s).

Funding

This work was funded by The Swedish Research Council (Grant 2016-04413). We gratefully acknowledge the financial supports from Kempestiftelserna (MA) and Stiftelsen Olle Engkvist Byggmästare (YJH).

References

[1] Komarneni S, Katsuki H. Microwave-hydrothermal synthesis of barium titanate under stirring condition. Ceram Int. 2010;36:1165–1169. DOI:10.1016/j.ceramint.2009.12.016.
[2] Xie B, Zhang Q, Zhang H, et al. Largely enhanced ferroelectric and energy storage performances of P(VDF-CTFE) nanocomposites at a lower electric field using $BaTiO_3$ nanowires by stirring hydrothermal method. Ceram Int. 2016;42:19012–19018. DOI:10.1016/j.ceramint.2016.09.057.
[3] Mourão HAJL, Lopes OF, Ribeiro C, et al. Rapid hydrothermal synthesis and PH-dependent photocatalysis of strontium titanate microspheres. Mater. Sci Semicond Process. 2015;30:651–657. DOI:10.1016/j.mssp.2014.09.022.
[4] Alnoor H, Chey CO, Pozina G, et al. Effect of precursor solutions stirring on deep level defects concentration and spatial distribution in low temperature aqueous chemical synthesis of zinc oxide nanorods. AIP Adv. 2015;5:087180. DOI:10.1063/1.4929981.
[5] Kuo CY, Ko RM, Tu YC, et al. Tip shaping for ZnO nanorods via hydrothermal growth of Zno nanostructures in a stirred aqueous solution. Cryst Growth Des. 2012;12:3849–3855. DOI:10.1021/cg2013182.
[6] Vediappan K, Guerfi A, Gariépy V, et al. Stirring effect in hydrothermal synthesis of nano C-LiFePO4. J Power Sourc. 2014;266:99–106. DOI:10.1016/j.jpowsour.2014.05.005.
[7] Jiang X, Jiang Y-B, Brinker CJ. Hydrothermal synthesis of monodisperse single-crystalline alpha-quartz nanospheres. Chem Commun. 2011;47:7524. DOI:10.1039/c1cc11115a.
[8] Matsumoto K, Hamana H, Iida H. Compendium of cycloaddition reactions under high pressure. Helv Chim Acta. 2005;88:2033–2234.
[9] Matsumoto K. Organic-synthesis under high-pressure. Synthesis (Mass). 1985;1:1–26.
[10] Andersson P, Bäckström G. Thermal conductivity of solids under pressure by the transient hot wire method. Rev Sci Instrum. 1976;47. DOI:10.1063/1.1134581.
[11] Shell Morlina S2 B 150 Industrial Bearing & Circulating Oils; 2014.
[12] Harris KR, Woolf LA. Temperature and volume dependence of the viscosity of water and heavy water at low temperatures. J Chem Eng Data. 2004;49:1064–1069. DOI:10.1021/je049918m.
[13] Kestin J, Sokolov M, Wakeham WA. Viscosity of liquid water in the range −8 °C to 150 °C. J Phys Chem Ref Data. 1978;7:941–948. DOI:10.1063/1.555581
[14] Abramson EH. Viscosity of water measured to pressures of 6 GPa and temperatures of 300°C. Phys Rev E. 2007;76:1–6. DOI:10.1103/PhysRevE.76.051203.
[15] Huber ML, Perkins RA, Laesecke A, et al. New international formulation for the viscosity of H_2O. J Phys Chem Ref Data. 2009;38:101–125. DOI:10.1063/1.3088050.
[16] Pistorius CWFT, Rapoport E, Clark JB. Phase diagrams of H_2O and D_2O at high pressures. J Chem Phys. 1968;48:5509–5514. DOI:10.1063/1.1668248.
[17] Krad I, Bidault O, Geoffroy N, et al. Preparation and characterization of $K_{0.5}Bi_{0.5}TiO_3$ particles synthesized by a stirring hydrothermal method. Ceram Int. 2016;42:3751–3756. DOI:10.1016/j.ceramint.2015.10.158.
[18] Demoisson F, Piolet R, Bernard F. Hydrothermal synthesis of ZnO crystals from $Zn(OH)_2$ metastable phases at room to supercritical conditions. Cryst Growth Des. 2014;14:5388–5396. DOI:10.1021/cg500407r.

[19] Moezzi A, Cortie M, McDonagh A. Aqueous pathways for the formation of zinc oxide nanoparticles. Dalt Trans. 2011;40:4871–4878. DOI:10.1039/c0dt01748e.
[20] Kolodziejczak-Radzimska A, Jesionowski T. Zinc oxide-from synthesis to application: a review. Materials (Basel). 2014;7:2833–2881. DOI:10.3390/ma7042833.
[21] Tietze L F, Steck P L. High pressure in organic synthesis: influence on selectivity. In: Van Eldik R, Klaner F-G., editors. High pressure chemistry: synthetic, mechanistic, and supercritical applications. Weinheim: Wiley-VCH Veriag GmbH; 2002. p. 239–283.
[22] Wurche F, Klärner FG. The effect of pressure on organic reactions: basic principles and mechanistic applications. High Press Chem Synth Mech. Supercrit. Appl. 2007: 41–96. DOI:10.1002/9783527612628.ch02.
[23] Chen B, Hoffmann R, Cammi R. The effect of pressure on organic reactions in fluids—a new theoretical perspective. Angew Chemie – Int Ed. 2017;56:11126–11142. DOI:10.1002/anie.201705427.